Proceedings of the ASME 2025
International Design Engineering Technical Conferences and
Computers and Information in Engineering Conference
IDETC-CIE2025
August 17-20, 2025, Anaheim, CA

DETC2025-168891

BANDGAP FORMATION MECHANISMS IN LOCALLY RESONANT METAMATERIALS WITH SPATIAL MODULATION

Joshua LeGrande,
Department of
Mechanical Engineering
Virginia Polytechnic Institute
and State University
Blacksburg, Virginia 24061

Mohammad Bukhari,
Department of
Mechanical Engineering
Wayne State University
Detroit, Michigan, 48202

Arun Malla, Oumar Barry*
Department of
Mechanical Engineering
Virginia Polytechnic Institute
and State University
Blacksburg, Virginia 24061

ABSTRACT

Metamaterials that make use of either topological patterning or local resonators have been vastly studied for their robust edge states, energy harvesting capabilities, and reconfigurability. However, these two metamaterials apply different bandgap formation mechanisms, and their joint dynamic interactions are not well defined. This work seeks to understand the formation of bandgaps in structures with spatially modulated resonators. Analysis is performed on a 1D spring-mass chain consisting of two cases of quasiperiodic modulation. In the first case, the main cell stiffness is modulated spatially, and in the second case, the resonator stiffness is modulated spatially. For both cases, the dispersion relation of the infinite chain is determined analytically, and confirmed by numerically calculating the eigenvalues of a finite chain. For both cases, an analytical dispersion relation is obtained for an infinite chain and validated numerically through eigenvalue analysis. By using the inverse method, the mechanisms behind bandgap formation are determined through the imaginary wavenumber components. The integrated density of states function is used to approximate the Chern number and confirm the topological nature of each bandgap. The mode shapes are also determined from the eigenvectors, revealing beneficial features for topological pumping. From this, it is shown that, for systems with modulated resonators, it is possible to alter both how many bandgaps exist and how those bandgaps are formed. Overall, the results reveal a rich and highly tunable band structure with many benefits over metamaterials with identical resonators.

1 INTRODUCTION

Metamaterials are carefully designed, man-made structures with unique configurations or material constituents that allow them to possess properties not found in nature [1, 2]. Metamaterials first emerged to control electromagnetic and optical wave propagation [3], but they can now be found in acoustic [4] and mechanical [5] applications as well. Their unique dynamic properties are useful for a wide array of applications including vibration and noise control [6], structural health monitoring [7], energy harvesting [8], cloaking [9], and mechanical computing [10].

These properties are often obtained by arranging unit cells in specific patterns including periodic patterns [1], quasiperiodic patterns [11], or even random configurations [12]. Periodic patterning, for example, produces bandgaps in the frequency response through a phenomena known as Bragg scattering. At frequencies within the bandgap, waves are reflected within the material and prevented from propagating [13–18]. However, these bandgaps are created at frequencies tied to the lattice constant of the metamaterial. Thus, their applications are often limited to structures with larger lattice constants or lower frequency vibra-

*Corresponding Author (Email: obarry@vt.edu)

tions [1].

Fortunately, local resonators have been introduced as a means to overcome this design requirement [19]. Structures with local resonators are capable of opening bandgaps over a much wider range of wavelengths than just those near the lattice constant. This is because locally resonant bandgaps are formed due to mode hybridization and appear near the natural frequency of the resonators rather than at wavelengths near to the lattice size [20]. Furthermore, Bragg scattering is not necessary for bandgap formation in the presence of local resonators. Therefore, locally resonant structures can still form bandgaps in random or aperiodic configurations [12].

Although locally resonant metamaterials are capable of improved vibration attenuation over periodic structures, their effectiveness is limited to frequencies near their design frequency. This has led to much work attempting to widen their operational frequency range. A common approach has been to include multiple resonators with distinct resonator frequencies in order to create multiple bandgaps at unique frequency ranges [6,21,22]. Another method has been to use different types of resonators such as bistable [23] or coupled resonators [24] to broaden the locally resonant bandgap. Adding a pattern to the resonators' spacing or parameters has also been effective for creating broader bandgaps or multiple bandgaps [25, 26]. Furthermore, the introduction of electromechanical elements, such as piezoelectric resonators, allows local resonators to be more adaptable. By coupling these electromechanical resonators to active circuits, it is possible to tailor the bandgap via the circuit parameters without altering the physical resonator parameters [27–30].

Spatially modulated metamaterials, such as those with quasiperiodic patterns, have also been shown to strengthen energy harvesting and vibration control by producing multiple bandgaps which host topologically protected edge modes. Periodic and locally resonant metamaterials are able to produce bandgaps that are topologically trivial, but quasiperiodic metamaterials can create multiple topologically robust bandgaps with vibration modes that are localized to lower dimensions [31]. These modes are formed passively by breaking spatial inversion symmetry while maintaining time-reversal symmetry [32–34]. This can be accomplished by modulating parameters within the structure following a quasiperiodic pattern, such as the Aubry-André model [35] as seen in [11, 36–42]. The frequency spectra of these patterned metamaterials resemble the Hofstadter butterfly [43] as they display multiple topological bandgaps where none exist in periodic structures. Furthermore, each topological bandgap is traversed by a topological edge mode which displays localized vibrations within finite structures [38]. The introduction of a phase variable in a second dimension allows for these edge modes to be pumped from one edge of the structure to the other [44–46].

Despite the superior dynamical properties of locally resonant metamaterials, few works have revealed their topological features through spatial modulation. The first proposed locally resonant quasiperiodic metamaterial introduces a quasiperiodic pattern to the spacing of resonators attached to a homogeneous beam [40]. The combined resonance and patterning effects result in a frequency spectrum that includes multiple topological bandgaps as well as one additional topologically trivial bandgap at the resonators' natural frequency. In [47], the main cells of a discrete chain are modulated in a quasiperiodic pattern with identical electromechanical resonators. This work demonstrates that weak electromechanical coupling has no impact on the topological features in the band structure. The ability to produce topological edge modes through resonator patterning is first studied experimentally in [48]. This work reveals the ability to create topological phenomena solely through the resonator parameters, allowing for topological features to be present in structures that need to maintain homogeneity in their core structure. Furthermore, combined spatial and temporal modulation of resonator parameters has been used to break reciprocity and produce one-way wave propagation [49, 50].

Despite these works, the combined effects of local resonance and spatial patterning are not well studied. No analytical study has explored the underlying methods of bandgap formation in metamaterials with modulated resonators, and thus, the design and tuning of these metamaterials is challenging. In this work, we study a topological metamaterial with quasiperiodic modulation in the resonator stiffness to examine the interactions between topological features and local resonance. The proposed metamaterial consists of a spring-mass chain in which each main cell hosts a single local resonator. Two cases of modulation patterning are considered, with modulation found in the main cell stiffness or resonator stiffness. An analytical dispersion relation is obtained for an infinite chain using a single unit cell. The band structures and mode shapes for finite chains are also obtained through eigenvalue analysis. The two cases are compared to observe the impact of modulation location and reveal multiple unique phenomena due to modulating resonator parameters. Furthermore, the inverse method and analysis of Chern number are used to characterize both the topological nature and formation mechanism of each bandgap.

2 MODELING AND SOLUTION METHODS

In this work, we consider a 1-dimensional locally resonant metamaterial shown in Fig. 1. The metamaterial consists of identical masses, m, connected by springs with stiffness, k, and coupled to local resonators with stiffness, k_r, and mass m_r. Multiple sources of spatial modulation are introduced including in the main cell stiffness and in the resonator stiffness. The modulated stiffness can be defined as

$$K_n = K_0[1 + \lambda cos(2\pi n\theta + \phi)] \tag{1}$$

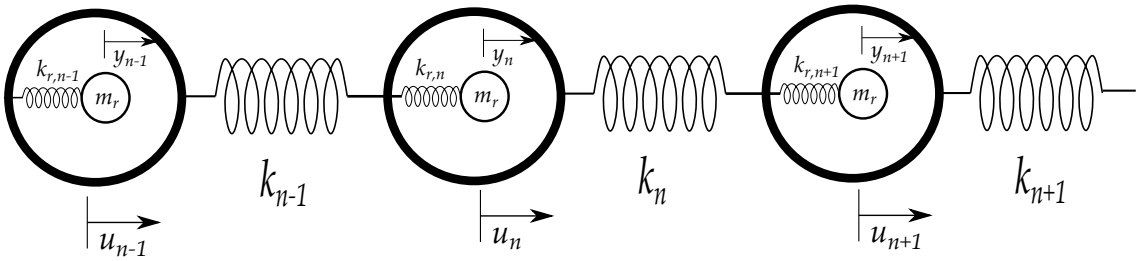

FIGURE 1: A diagram of the quasiperiodic metamaterial with variation in the stiffness of the main cells or resonators.

where, in this case, K_n may refer to either the main cell or resonator stiffness of the n^{th} element. K_0 is the average stiffness, and λ is the modulation amplitude. This pattern, known as the Aubry-André Model [35], is defined by the quasiperiodic parameter, θ, and phase variable, ϕ. The governing equations of motion for the n^{th} mass and resonator are

$$m\ddot{u}_n + k_{n-1}(u_n - u_{n-1}) + k_n(u_n - u_{n+1}) + k_{r,n}(u_n - y_n) = 0 \quad (2)$$

$$m_r\ddot{y}_n + k_{r,n}(y_n - u_n) = 0 \quad (3)$$

for the displacement of the n^{th} mass, u_n, and resonator, y_n. We impose a Bloch periodic solution of

$$u_n = \bar{U}_n e^{i(\mu n - \omega t)} \qquad y_n = \bar{Y}_n e^{i(\mu n - \omega t)} \quad (4)$$

with mass and resonator displacement amplitudes, $\bar{U}_n$ and $\bar{Y}_n$, frequency, ω, time, t, and non-dimensional wavenumber μ. Plugging these solutions in yield new governing equations

$$\begin{aligned}&(-m\omega^2 + k_{n-1} + k_n + k_{r,n})\bar{U}_n - k_{n-1}\bar{U}_{n-1}e^{-i\mu} \\ &-k_n\bar{U}_{n+1}e^{i\mu} - k_{r,n}\bar{Y}_n = 0\end{aligned} \quad (5)$$

$$(-m_r\omega^2 + k_{r,n})\bar{Y}_n - k_{r,n}\bar{U}_n = 0 \quad (6)$$

These equations provide an analytical frequency-wavenumber relationship in the form of an eigenvalue problem which can be used to obtain the dispersion relations through modal analysis. By modeling a single unit cell, the dispersion relations for an infinite system are revealed. Additionally, the inverse method is used to obtain both parts of the complex wavenumber. To further validate the analytical dispersion relations, the eigenvalues and eigenvectors are calculated for a finite chain, yielding the natural frequencies and mode shapes, respectively, over the full range of phase variable, ϕ.

3 RESULTS

To fully reveal how local resonators and spatial modulation work together to form bandgaps, we will consider two cases. The first case will have modulation in the main cell stiffness, and the second case will have modulation in the resonator stiffness. We will study both infinite chains and finite chains with 60 cells. The quasiperiodic parameter will be $\theta = 1/4$, which will create a pattern that repeats every four cells. The other system parameters will be as follows: $m = 1$ kg, $k_0 = 1$ N/m, $m_r = 0.2$ kg, $k_{r,0} = 0.3$ N/m, and $\lambda = 0.6$. The phase angle, ϕ, will range from 0 to 2π. For the parameters that vary in space, the subscript 0 indicates an average value.

In this section, we will determine how the interactions between local resonance and spatial modulation impact the band structure and mode shapes in both cases. We will first compare the dispersion relations and band structures for both cases to reveal how the location of patterning causes different bandgaps to form. From there, the mode shapes will be used to reveal unique properties introduced through resonator modulation.

3.1 Effect of Modulated Parameter

Using the inverse method, the real and imaginary components of the wavenumber are determined as a function of frequency for both cases in Fig. 2. The frequency displayed here, Ω, is nondimensional such that $\Omega = \omega/\omega_0$ where $\omega_0 = \sqrt{k_0/m}$. The real components of the wavenumber are shown on the right side of each figure in black, and the imaginary components of the wavenumber are shown on the left in red. The resonator's natural frequencies are $w_{r,n} = \sqrt{k_{r,n}/m_r}$ and appear in the figure as dashed blue lines. When looking just at the real components, the two cases yield similar dispersion curves. The eight roots of the characteristic equation produce eight passbands separated by seven bandgaps, regardless of which parameter is modulated.

Although changing the parameter being modulated does not impact the number of bandgaps, it can still significantly alter their behavior. Previously, Gao and Wang [22] reported that, with multiple distinct resonators, it is possible to couple local resonance and Bragg scattering within a single bandgap that displays the behavior of both. To reveal which method is being used to open each bandgap, we use the imaginary wavenum-

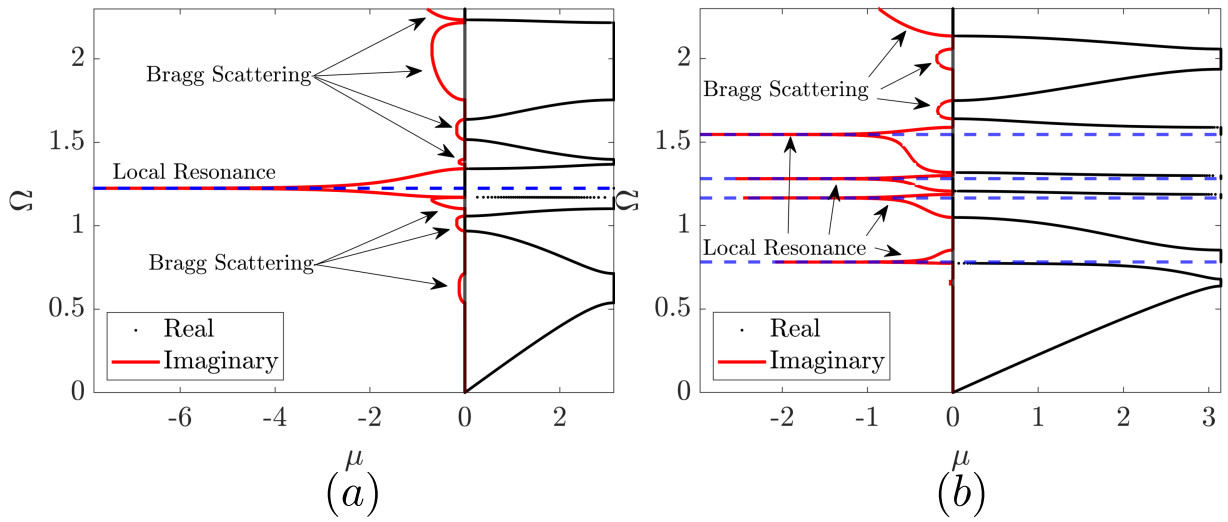

FIGURE 2: Dispersion relations for varying stiffness in the (a) main cells (case 1), and (b) resonators (case 2), at phase, $\bar{\phi} = 0.8\pi$. The mechanism behind each bandgap is labeled. The dashed blue lines indicate the frequencies of the resonators.

ber components and criteria outlined by Liu and Hussein [20]. Using their criteria, Bragg scattering bandgaps yield attenuation zones with imaginary components that are nearly semi-circular while locally resonant bandgaps display much stronger peaks centered at the natural frequency of the resonator. Case 1, shown in Fig. 2(a), has identical resonators and thus, a single locally resonant bandgap. Each of the remaining bandgaps are created via Bragg scattering. However, for case 2, there are four locally resonant frequencies, each of which create a locally resonant bandgap centered on their frequency. It is important to note that the magnitude of the imaginary component of the wavenumber is directly tied to the strength of vibration attenuation. With this in mind, varying the resonator stiffness provides the opportunity to significantly improve vibration attenuation performance over a wider frequency range.

While the passbands do not display significant changes with variations in the wavenumber, varying the phase angle, ϕ, may uncover further differences. Furthermore, varying the phase angle often reveals meaningful topological trends in finite structures, such as topological pumping, which will be seen in the next section. For this reason, the band structures are plotted for finite and infinite chains in Fig. 3 for both cases. The gray background represents the bulk passbands of the infinite chain while the natural frequencies of the finite chain appear as black lines. Additionally, multiple modes that span the bandgaps are indicated in red, and the dashed blue lines again represent the resonators' natural frequencies. As mentioned before, both cases display eight passbands and seven bandgaps. In the first case, shown in Fig. 3(a), six bandgaps are spanned by a topological edge mode, while one bandgap is not. Prior work has revealed that the fourth (locally resonant) bandgap is topologically trivial and does not contain an edge mode. Meanwhile, each of the other bandgaps are topologically non-trivial with edge modes present [47]. The topologically trivial bandgap is located at the single natural frequency of the resonators, and it divides the passbands equally with four above and below.

When the modulation is moved to the resonator stiffness, shown in Fig. 3(b), there are multiple resonator frequencies. In this specific example, with $\theta = 1/4$, there are four. The presence of multiple resonator frequencies here results in some major changes to the band structure, and it is crucial to determine how these changes impact bandgap formation. Because there is more than one resonator frequency, we cannot only consider individual resonator frequencies. Instead. we must consider the entire range of resonator frequencies. The effects of modulating the resonator stiffness primarily occur within this range, which can be visualized in Fig. 3(b) as the frequency range bounded by the uppermost and lowest dashed blue lines.

Within this resonator frequency range, the passbands are much more sensitive to changes in the phase angle, ϕ, showing much greater fluctuation in Fig. 3(b). Even the central (fourth) bandgap, which is constant for case 1, shows some variation in case 2. More significantly, there exist multiple points in the band structure at which some passbands get progressively narrower until they disappear altogether. At these points, the two adjacent band gaps merge into one. These points can be found at phase angles where one of the resonator frequencies cross the passband. The passband shrinks as the resonator frequency approaches it, and, for a moment, it disappears when the frequency of the resonator aligns with the frequency of the passband. This can be seen, for example, in Fig. 3(b) at phase $\bar{\phi} = 0.83\pi$ where the fourth passband disappears as a resonator frequency moves from

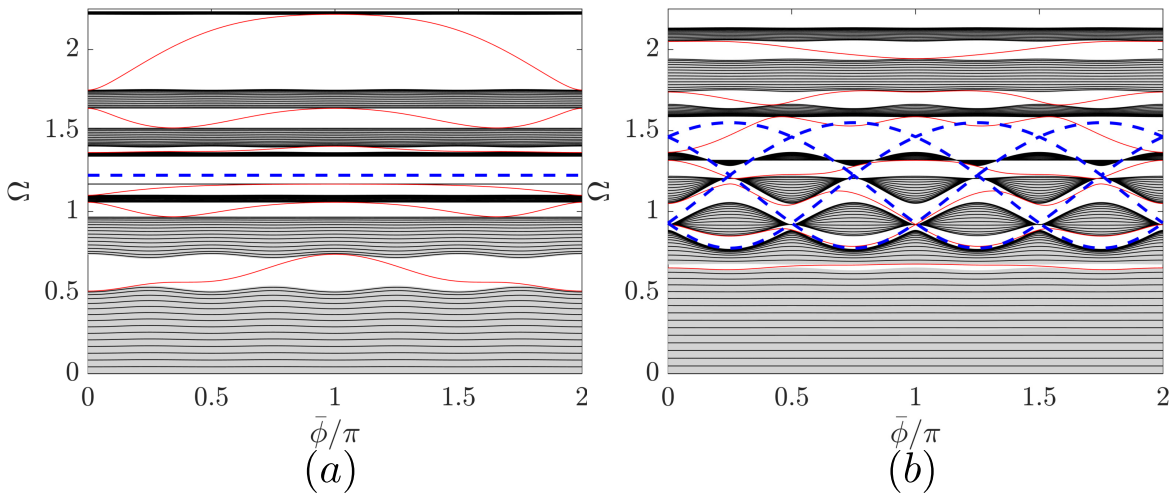

FIGURE 3: Natural frequencies of a finite chain with 60 cells with modulation in the stiffness of the (a) main cells (case 1) and (b) resonators (case 2). The finite eigennfrequencies are shown as black lines while the bulk passbands of the infinite chain are shown as the gray background. Edge modes and resonator frequencies are highlighted in red and blue, respectively.

the fourth bandgap up to the third, and the two bandgaps merge. This indicates for the first time that, with modulated resonators, it is possible to control how many passbands exist in a spatially modulated system without directly changing the modulation pattern. For example, there have always been eight passbands and seven bandgaps in a locally resonant system with a modulation parameter of $\theta = 1/4$. However, now it is possible, through a careful selection of phase variable, to produce seven passbands and six bandgaps in the same structure.

During these critical transitions, the natural frequency of one resonator traverses into a different bandgap, which usually hosts a second resonator frequency already. When the resonator frequency leaves one bandgap and enters another, it also changes the nature of both bandgaps. To study this further, we will take a closer look at the imaginary components of the wavenumber at multiple phase angles during this transition. These are shown in Fig. 4 for the previously mentioned crossing point at $\bar{\phi} = 0.83\pi$. Fig. 4(a) displays a zoomed in view of the fourth passband for case two along with both wavenumber components at the crossing point in Fig. 4(b) and the imaginary components at three other points of interest in Fig. 4(c)-(e). At point I, in Fig. 4(c), there are two distinct bandgaps formed by local resonance since both resonator frequencies are in separate bandgaps. However, at point II, in Fig. 4(b), the passband is overlapped exactly by the resonator frequency, causing it to disappear. Looking at the real component of the wavenumber, this passband has vanished entirely from the dispersion relation. Furthermore, we can see from looking at the imaginary components that the peak in attenuation at the resonator frequency has also vanished. The resulting bandgap displays both the width typical of a Bragg scattering bandgap and the attenuation peak common in locally resonant bandgaps. As we look further in the transition to point III, shown in Fig. 4(d), two distinct bandgaps appear again, but the nature of the lower bandgap has changed. Since there is no longer a resonator frequency within the bandgap, the lower (third) bandgap is now formed via Bragg scattering only. Meanwhile, two attenuation peaks exist within the fourth bandgap at the frequencies of the two resonators. Eventually at point IV, in Fig. 4(e), the two peaks merge into a single resonant peak when the resonator frequencies converge. This transition reveals that, by varying the phase angle alone, it is possible to not only control the number of bandgaps, but also which formation mechanisms, Bragg scattering or local resonance, open each bandgap.

One further distinction to make between the cases with resonators that are identical or varying is the existence of one more mode spanning the fourth bandgap. For the case with identical resonators, in Fig. 3(a), we have already determined that the fourth bandgap is topologically trivial and hosts no edge modes. However, when the resonator stiffness is modulated in Fig. 3(b), there is a mode within the fourth bandgap. The presence of this mode calls into question whether this bandgap remains topologically trivial. To address this, the Chern number will be used to determine which bandgaps are topological or trivial. The Chern number is a topological invariant that defines the topological nature of bandgaps, and the bulk-boundary correspondence principle relates the Chern number to the presence of edge modes within bandgaps [51]. For each bandgap, a nonzero Chern number indicates a topological bandgap, and it ensures the presence of an edge mode spanning the bandgap. Direct computation of the Chern number can be arduous, so in this study, it is approximated using the Integrated Density of States (IDS) function following the method outlined in [37]. The IDS at a frequency, Ω,

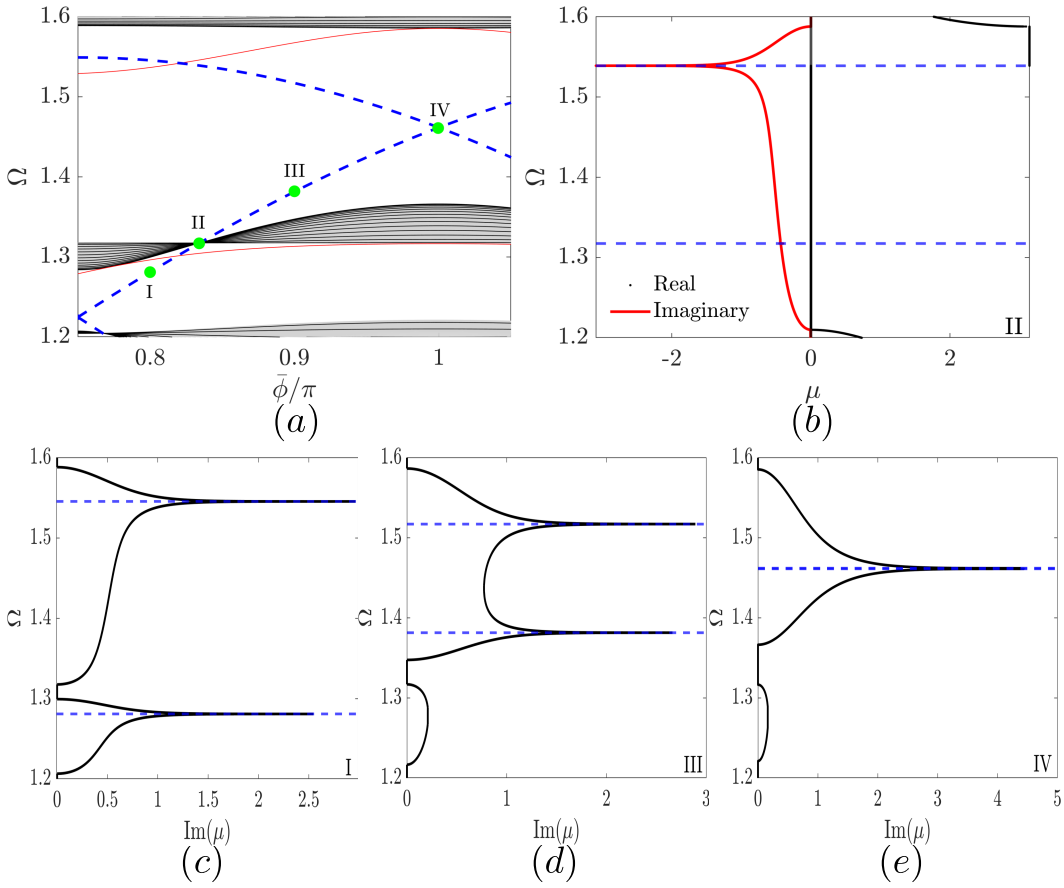

FIGURE 4: (a) Band structure with modulated resonators (case 2) from Fig. 3(b), showing the collapse of the fifth passband. Significant points are marked at $\bar{\phi} = 0.8\pi$, 0.8344π, 0.9π, and 0.995π. (b) Wavenumber components at $\bar{\phi} = 0.8344\pi$ when the fifth passband disappears. (c)-(e) Imaginary wavenumber components at other points indicating a change in bandgap formation mechanisms. The dashed blue lines represent frequencies of resonators.

is defined as

$$\mathrm{IDS}(\Omega) = \lim_{N\to\infty} \frac{\sum_n [\omega_n \leq \Omega]}{N} \tag{7}$$

where ω_n is the n$^{\text{th}}$ natural frequency, and $[\cdot]$ are the Iverson brackets returning a value of 1 when the enclosed statement is true and a value of 0 if it is false. Put simply, this function counts the number of natural frequencies at or below a frequency, Ω, and normalizes it to the size of the chain, N. Theoretically, this value will converge as the chain nears an infinite length, but for practicality, we will consider here a long chain with $N = 1000$ masses.

The IDS function is plotted for both cases in Fig. 5 while sweeping the modulation parameter, θ fully from 0 to 1. In this representation, the colormap indicates the frequency, and the lines of distinct shifts in color mark the bandgaps. The sharp changes in color occur where there is a significant change in frequency between two states in the system since all frequencies within a bandgap have the same IDS value. The equation for these lines can be expressed as

$$\mathrm{IDS}(\theta) = a + b\theta \tag{8}$$

with intercept, a, and slope, b. From Streda's formula, $\frac{\partial \mathrm{IDS}}{\partial \theta} = C_g$, we know that the Chern number labeling each bandgap, C_g, is equal to the slope of that bandgap's line in the IDS plot. Some significant bandgaps are emphasized in Fig. 5 using dashed white lines alongside the equation for each bandgap. For both cases, there is a single horizontal line at the frequency of the fourth bandgap. Meanwhile, each of the other bandgaps have a nonzero slope. This indicates that the fourth bandgap is still topologically trivial while each of the other bandgaps remain topological. More significantly, this reveals that the parameter being modulated has no impact on the topological nature of the bandgaps.

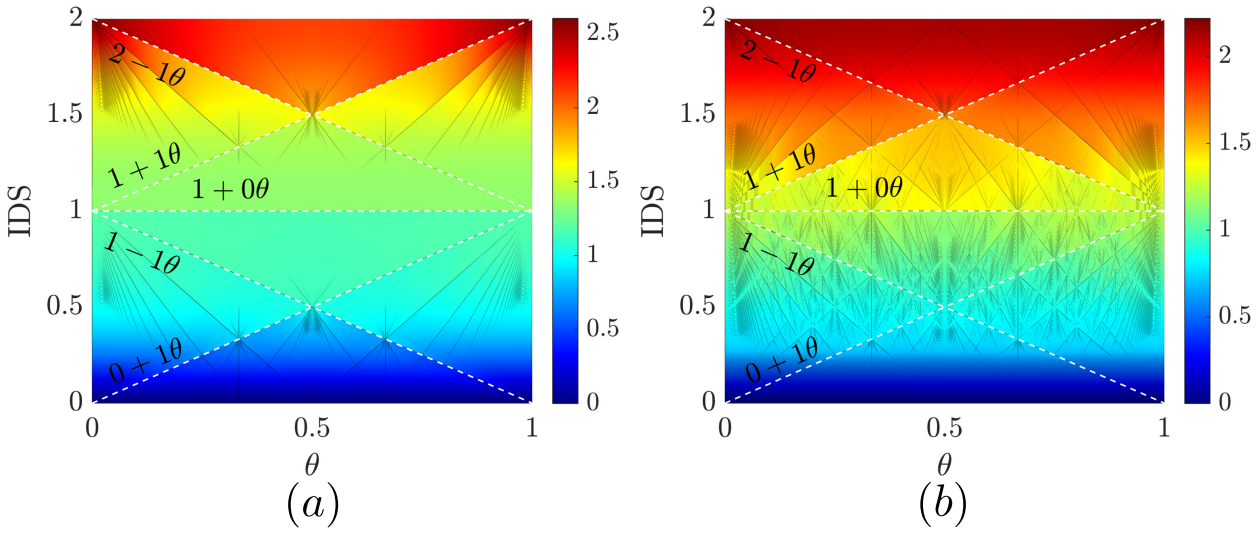

FIGURE 5: Integrated Density of States (IDS) as a function of the quasiperiodic parameter, θ, at $\bar{\phi} = 0$ for modulation in the stiffness of the (a) main cells (case one) and (b) resonators (case two). White dashed lines and corresponding equations indicate some bandgaps.

3.2 Mode Shapes

Modulating the resonator stiffness strongly affects the band structure, but these changes also have an impact on the mode shapes. By observing the band structure, we see an extra mode appearing within the trivial bandgap along with some noteworthy alterations to a few of the pre-existing edge modes. The impact of these changes can be determined through the mode shapes. When exciting a finite chain at a mode within one of its topological bandgaps, the vibration response will be localized to the edge. This phenomena has been previously reported in multiple studies for the case with modulation in the main cells, so a thorough discussion of these edge modes will be withheld here. Instead, this discussion will focus on the two unique characteristics that are brought about by modulating the resonator stiffness.

First, there is the presence of a mode within the topologically trivial (fourth) bandgap, as previously mentioned. To help visualize how this mode traverses the bandgap, Fig. 6(a) shows a zoomed in band structure emphasizing the fourth and fifth bandgaps of case 2. By plotting the mode shape for the fourth bandgap in Fig. 6(b), the existence of this edge mode is confirmed. Here, a 60 cell chain is excited at the frequency of the mode within the fourth bandgap while sweeping the phase variable by a full 2π cycle. The mode shape is also normalized to the maximum displacement for better visualization. Although this bandgap has been shown to be topologically trivial, the mode shape is still edge-localized, and it behaves similarly to the other edge modes. Like the other edge modes, this mode frequency begins on one passband and, as ϕ is varied, it leaves the passband and enters the bandgap. Eventually, it makes contact with the other passband and crosses the gap again, returning to the original passband. The mode shape reflects the effect of this transition in Fig. 6(b). Every time the mode frequency touches one of the passbands, even momentarily, the localization switches to the opposite edge.

The second significant impact is that modulating resonator parameters can lead to multiple edge modes that make contact with the passbands more frequently. Generally, an edge mode will make contact with one passband, and then span the bandgap to touch the opposite passband. Whenever the edge mode frequency contacts one of the passbands, the edge localization switches from one edge to the opposite. However, some edge modes behave differently when the resonator stiffness is modulated. In some bandgaps, an edge mode frequency may make contact with a single passband multiple times consecutively. Two clear examples of this can be seen within the fourth and fifth bandgaps, highlighted in Fig. 6(a). For the fifth bandgap, the edge mode is in contact with the fifth passband at $\bar{\phi} = 0$ and then makes contact with the sixth passband three times at $\bar{\phi} = 0.46\pi$, π, and 1.54π before returning to the fifth passband at $\bar{\phi} = 2\pi$. The mode shape associated with this mode is shown in Fig. 6(c). Each time the mode frequency makes contact with a passband, the localized mode migrates from one end of the structure to the opposite. The additional points of contact with the sixth passband result in more frequent edge-to-edge transitions for the mode shape. This can be useful for topological pumping applications where the phase is being varied temporally or spatially. Normally, a full pumping cycle would require the phase angle to be varied by the full range of 2π, but in this case, the phase only needs to be varied by π.

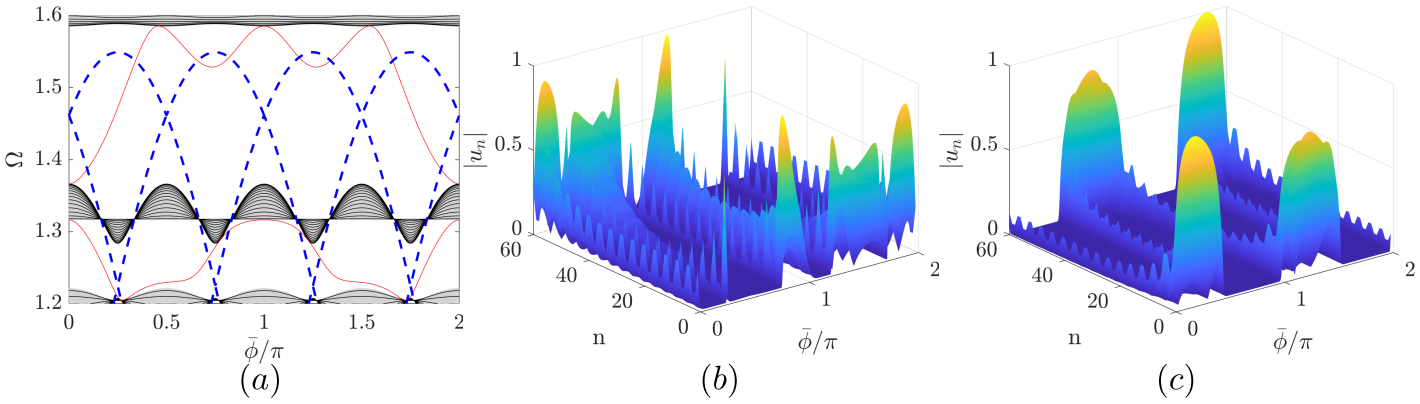

FIGURE 6: (a) Zoomed in band structure with modulated resonators (case 2) showing the additional modes within the fourth and fifth bandgaps. (b)-(c) Displacement mode shapes with variation in the phase angle, $\bar{\phi}$, for case 2 with excitation of the fourth and fifth edge modes, respectively.

4 CONCLUSION

In this study, we explored how the combined effects of spatial modulation and local resonance formed bandgaps in a single metamaterial. The metamaterial under consideration was modeled as a 1-dimensional spring mass chain with a single local resonator within each main cell. Two cases of modulation were considered with spatial modulation in either the main cell stiffness or resonator stiffness. Through analysis of the unit cell, an analytical dispersion relationship was obtained for an infinite chain. This relationship was then validated numerically through eigenvalue analysis of a finite chain. The mode shapes of the finite chain were also determined from the eigenvectors. Furthermore, we investigated how changing the modulated parameter impacted both how the bandgaps were formed and whether they were topological or trivial.

The results indicated that modulating the resonator stiffness instead of the main cell stiffness yields a more complex and highly tunable band structure with many unique features. When the resonator stiffness was modulated, multiple locally resonant bandgaps were formed in the place of bandgaps that were previously formed via Bragg scattering, leading to improved vibration attenuation performance. The presence of multiple resonator frequencies also created stronger fluctuations in the passbands with variation in the phase angle. At multiple points, some passbands collapsed fully as the adjacent bandgaps merged into one. During this transition, as the passband closed and reopened, the adjacent bandgaps also transitioned from locally resonant bandgaps back to Bragg scattering bandgaps. These transition points indicated, for the first time, the ability to control both the number and type of bandgaps in a metamaterial without altering the modulation parameter. Additionally, modulating the resonator parameter produced an extra edge mode in the topologically trivial bandgap that hosted no edge modes previously. Calculating the Chern number through the integrated density of states function revealed that this bandgap remained topologically trivial and that the parameter being modulated does not alter the topological nature of any bandgap. Furthermore, we observed select mode shapes that pump waves from one edge to the other over a shorter phase cycle.

Overall, metamaterials with spatial modulation in their resonators have been shown to have many beneficial features over metamaterials with modulation in their main cells. These metamaterials possess band band structures that are more highly tunable via resonator and patterning parameters. Studying the mode shapes has also confirmed the existence of one more edge mode capable of topological pumping. Because these benefits depend on the resonator parameters, they may be inserted into non-resonant systems regardless of their outer patterning or structure. Furthermore, this facilitates the possibility for highly reconfigurable metamaterials with a range of applications including topological pumping, wave guiding, breaking reciprocity, and energy harvesting.

ACKNOWLEDGEMENTS

This work is supported in part by the National Science Foundation (NSF) Grant CMMI-2038187.

REFERENCES

[1] Hussein, M. I., Leamy, M. J., and Ruzzene, M., 2014. "Dynamics of phononic materials and structures: Historical origins, recent progress, and future outlook". *Applied Mechanics Reviews,* ***66***(4), p. 040802.

[2] Bertoldi, K., Vitelli, V., Christensen, J., and van Hecke, M., 2017. "Flexible mechanical metamaterials". *Nature Reviews Materials,* ***2***(11), p. 17066.

[3] Cai, W., and Shalaev, V. M., 2010. *Optical Metamaterials*, Vol. 10. Springer.
[4] Martínez-Sala, R., Sancho, J., Sánchez, J. V., Gómez, V., Llinares, J., and Meseguer, F., 1995. "Sound attenuation by sculpture". *Nature,* ***378***(6554), pp. 241–241.
[5] Christensen, J., Kadic, M., Kraft, O., and Wegener, M., 2015. "Vibrant times for mechanical metamaterials". *MRS Communications,* ***5***(3), pp. 453–462.
[6] Zhu, R., Liu, X., Hu, G., Sun, C., and Huang, G., 2014. "A chiral elastic metamaterial beam for broadband vibration suppression". *Journal of Sound and Vibration,* ***333***(10), pp. 2759–2773.
[7] Lu, Z., Wang, Z., Zhou, Y., and Lu, X., 2018. "Nonlinear dissipative devices in structural vibration control: A review". *Journal of Sound and Vibration,* ***423***, pp. 18–49.
[8] Li, Y., Baker, E., Reissman, T., Sun, C., and Liu, W. K., 2017. "Design of mechanical metamaterials for simultaneous vibration isolation and energy harvesting". *Applied Physics Letters,* ***111***(25), p. 251903.
[9] Darabi, A., Zareei, A., Alam, M.-R., and Leamy, M. J., 2018. "Experimental demonstration of an ultrabroadband nonlinear cloak for flexural waves". *Physical Review Letters,* ***121***(17), p. 174301.
[10] Zangeneh-Nejad, F., Sounas, D. L., Alù, A., and Fleury, R., 2021. "Analogue computing with metamaterials". *Nature Reviews Materials,* ***6***(3), pp. 207–225.
[11] Rosa, M. I., Pal, R. K., Arruda, J. R., and Ruzzene, M., 2019. "Edge states and topological pumping in spatially modulated elastic lattices". *Physical Review Letters,* ***123***(3), p. 034301.
[12] Achaoui, Y., Laude, V., Benchabane, S., and Khelif, A., 2013. "Local resonances in phononic crystals and in random arrangements of pillars on a surface". *Journal of Applied Physics,* ***114***(10), p. 104503.
[13] Sigalas, M. M., and Economou, E. N., 1992. "Elastic and acoustic wave band structure". *Journal of Sound and Vibration,* ***158***, pp. 377–382.
[14] Sigalas, M., and Economou, E. N., 1993. "Band structure of elastic waves in two dimensional systems". *Solid State Communications,* ***86***(3), pp. 141–143.
[15] Kushwaha, M. S., Halevi, P., Dobrzynski, L., and Djafari-Rouhani, B., 1993. "Acoustic band structure of periodic elastic composites". *Physical Review Letters,* ***71***(13), p. 2022.
[16] Kushwaha, M. S., Halevi, P., Martinez, G., Dobrzynski, L., and Djafari-Rouhani, B., 1994. "Theory of acoustic band structure of periodic elastic composites". *Physical Review B,* ***49***(4), p. 2313.
[17] Vasseur, J., Djafari-Rouhani, B., Dobrzynski, L., Kushwaha, M., and Halevi, P., 1994. "Complete acoustic band gaps in periodic fibre reinforced composite materials: the carbon/epoxy composite and some metallic systems". *Journal of Physics: Condensed Matter,* ***6***(42), p. 8759.
[18] Kushwaha, M. S., 1996. "Classical band structure of periodic elastic composites". *International Journal of Modern Physics B,* ***10***(09), pp. 977–1094.
[19] Liu, Z., Zhang, X., Mao, Y., Zhu, Y., Yang, Z., Chan, C. T., and Sheng, P., 2000. "Locally resonant sonic materials". *Science,* ***289***(5485), pp. 1734–1736.
[20] Liu, L., and Hussein, M. I., 2012. "Wave motion in periodic flexural beams and characterization of the transition between bragg scattering and local resonance". *Journal of Applied Mechanics,* ***79***(1), p. 011003.
[21] Huang, G., and Sun, C., 2010. "Band gaps in a multiresonator acoustic metamaterial". *Journal of Vibration and Acoustics,* ***132***(3), p. 031003.
[22] Gao, Y., and Wang, L., 2020. "Ultrawide coupled bandgap in hybrid periodic system with multiple resonators". *Journal of Applied Physics,* ***127***(20).
[23] Xia, Y., Ruzzene, M., and Erturk, A., 2019. "Dramatic bandwidth enhancement in nonlinear metastructures via bistable attachments". *Applied Physics Letters,* ***114***(9), p. 093501.
[24] Hu, G., Tang, L., and Das, R., 2018. "Internally coupled metamaterial beam for simultaneous vibration suppression and low frequency energy harvesting". *Journal of Applied Physics,* ***123***(5), p. 055107.
[25] Meng, H., Chronopoulos, D., Fabro, A., Elmadih, W., and Maskery, I., 2020. "Rainbow metamaterials for broadband multi-frequency vibration attenuation: Numerical analysis and experimental validation". *Journal of Sound and Vibration,* ***465***, p. 115005.
[26] Alshaqaq, M., and Erturk, A., 2020. "Graded multifunctional piezoelectric metastructures for wideband vibration attenuation and energy harvesting". *Smart Materials and Structures,* ***30***(1), p. 015029.
[27] Yi, K., and Collet, M., 2021. "Broadening low-frequency bandgaps in locally resonant piezoelectric metamaterials by negative capacitance". *Journal of Sound and Vibration,* ***493***, p. 115837.
[28] Casadei, F., Delpero, T., Bergamini, A., Ermanni, P., and Ruzzene, M., 2012. "Piezoelectric resonator arrays for tunable acoustic waveguides and metamaterials". *Journal of Applied Physics,* ***112***(6), p. 064902.
[29] Thorp, O., Ruzzene, M., and Baz, A., 2001. "Attenuation and localization of wave propagation in rods with periodic shunted piezoelectric patches". *Smart Materials and Structures,* ***10***(5), p. 979.
[30] Bergamini, A., Delpero, T., Simoni, L. D., Lillo, L. D., Ruzzene, M., and Ermanni, P., 2014. "Phononic crystal with adaptive connectivity". *Advanced Materials,* ***26***(9), pp. 1343–1347.
[31] Ma, G., Xiao, M., and Chan, C. T., 2019. "Topological phases in acoustic and mechanical systems". *Nature Re-*

views Physics, ***1***(4), pp. 281–294.

[32] Mousavi, S. H., Khanikaev, A. B., and Wang, Z., 2015. "Topologically protected elastic waves in phononic metamaterials". *Nature Communications,* ***6***(1), pp. 1–7.

[33] Miniaci, M., Pal, R., Morvan, B., and Ruzzene, M., 2018. "Experimental observation of topologically protected helical edge modes in patterned elastic plates". *Physical Review X,* ***8***(3), p. 031074.

[34] Chaunsali, R., Chen, C.-W., and Yang, J., 2018. "Subwavelength and directional control of flexural waves in zone-folding induced topological plates". *Physical Review B,* ***97***(5), p. 054307.

[35] Aubry, S., and André, G., 1980. "Analyticity breaking and anderson localization in incommensurate lattices". *Ann. Israel Phys. Soc,* ***3***(133), p. 18.

[36] Apigo, D. J., Qian, K., Prodan, C., and Prodan, E., 2018. "Topological edge modes by smart patterning". *Physical Review Materials,* ***2***(12), p. 124203.

[37] Ni, X., Chen, K., Weiner, M., Apigo, D. J., Prodan, C., Alù, A., Prodan, E., and Khanikaev, A. B., 2019. "Observation of hofstadter butterfly and topological edge states in reconfigurable quasi-periodic acoustic crystals". *Communications Physics,* ***2***(1), pp. 1–7.

[38] Pal, R. K., Rosa, M. I., and Ruzzene, M., 2019. "Topological bands and localized vibration modes in quasiperiodic beams". *New Journal of Physics,* ***21***(9), p. 093017.

[39] Pu, X., Palermo, A., and Marzani, A., 2022. "Topological edge states of quasiperiodic elastic metasurfaces". *Mechanical Systems and Signal Processing,* ***181***, p. 109478.

[40] Xia, Y., Erturk, A., and Ruzzene, M., 2020. "Topological edge states in quasiperiodic locally resonant metastructures". *Physical Review Applied,* ***13***(1), p. 014023.

[41] Rosa, M. I., Leamy, M. J., and Ruzzene, M., 2023. "Amplitude-dependent edge states and discrete breathers in nonlinear modulated phononic lattices". *New Journal of Physics,* ***25***(10), p. 103053.

[42] LeGrande, J., Bukhari, M., and Barry, O., 2022. "Topological properties and localized vibration modes in quasiperiodic metamaterials with electromechanical local resonators". In International Design Engineering Technical Conferences and Computers and Information in Engineering Conference, Vol. 86311, American Society of Mechanical Engineers, p. V010T10A004.

[43] Hofstadter, D. R., 1976. "Energy levels and wave functions of bloch electrons in rational and irrational magnetic fields". *Physical Review B,* ***14***(6), p. 2239.

[44] Riva, E., Casieri, V., Resta, F., and Braghin, F., 2020. "Adiabatic pumping via avoided crossings in stiffness-modulated quasiperiodic beams". *Physical Review B,* ***102***(1), p. 014305.

[45] Riva, E., Rosa, M. I., and Ruzzene, M., 2020. "Edge states and topological pumping in stiffness-modulated elastic plates". *Physical Review B,* ***101***(9), p. 094307.

[46] Xia, Y., Riva, E., Rosa, M. I., Cazzulani, G., Erturk, A., Braghin, F., and Ruzzene, M., 2021. "Experimental observation of temporal pumping in electromechanical waveguides". *Physical Review Letters,* ***126***(9), p. 095501.

[47] LeGrande, J., Bukhari, M., and Barry, O., 2023. "Effect of electromechanical coupling on locally resonant quasiperiodic metamaterials". *AIP Advances,* ***13***(1), p. 015112.

[48] Rosa, M. I., Guo, Y., and Ruzzene, M., 2021. "Exploring topology of 1d quasiperiodic metastructures through modulated lego resonators". *Applied Physics Letters,* ***118***(13), p. 131901.

[49] Chen, Y., Li, X., Nassar, H., Norris, A. N., Daraio, C., and Huang, G., 2019. "Nonreciprocal wave propagation in a continuum-based metamaterial with space-time modulated resonators". *Physical Review Applied,* ***11***(6), p. 064052.

[50] Attarzadeh, M., Callanan, J., and Nouh, M., 2020. "Experimental observation of nonreciprocal waves in a resonant metamaterial beam". *Physical Review Applied,* ***13***(2), p. 021001.

[51] Hatsugai, Y., 1993. "Chern number and edge states in the integer quantum hall effect". *Physical review letters,* ***71***(22), p. 3697.